2009 IEEE International Conference on Robotics and Automation
Kobe International Conference Center
Kobe, Japan, May 12-17, 2009

Development of High-Sensitivity Slip Sensor Using Special Characteristics of Pressure Conductive Rubber

Seiichi Teshigawara*, Kenjiro Tadakuma*, Aiguo Ming*, Masatoshi Ishikawa**, Makoto Shimojo*

Abstract— **Even with the eyes closed, humans are able to grip an object with minimal force without such information as the coefficient of friction or the weight. Tactile sensors capable of detecting slippage are necessary for this gripping action to be realized in a robot hand. Heretofore, many slip sensors were developed and produced, but there was not a slip sensor of simple structure practical for installation on fingertips of a robot hand. Therefore, we propose a low-profile/lightweight slip sensor of simple structure. The special properties of pressure conductive rubber are utilized as a detection device in this sensor. In this paper, we discuss the results of trial manufacture and of slip detection property testing of this sensor. Moreover, we will report the results of slip prevention experiments by this prototype slip sensor, and indicate that the pressure conductive rubber is promising as a material of slip sensor.**

I. INTRODUCTION

In regard to the five senses of a human, practical sensors have been already developed to give robots the senses of sight and hearing. But, these alone, a robot cannot use tools skillfully; this is the special characteristics of a human. In order for robots to perform actions in place of human hands, tactile sensors that allow the acquisition of sensory information such as pressure, slippage, and temperature are necessary. Sensing of slippage plays an especially important role in the performance of gripping and manipulating objects.

Johansson et al. [1][2], in their research regarding the gripping motion of humans, made clear that humans grip objects at the minimum gripping force that is close to producing slip. It was also shown that the initial slip between the skin and the gripping object was essential to this sense. Therefore, up until now various slip sensors detecting initial slip have been proposed. Trembley et al. [3] developed a sensor, arranging acceleration sensors in sets of two inside a spherical silicon rubber with a projection called a "nib", that detected the vibrations which occur on the surface of the sensor as a result of initial slip. Son et al. [4] developed a sensor with four sheets of PVDF film arranged in a semi-circular silicon rubber tube that similarly detected the vibrations occurring from initial slip. Adding to the findings of Johansson et al., Maeno et al. [5] modelled the structure of the finger pad by means of finite element analysis and made clear the properties of individual tactile receptors. They then imitated the human gripping technique, developing sensors lined up inside a curved elastic surface at regular intervals along a strain gauge [6]. With this, they showed that it was possible to grip an object of unknown weight and coefficient of friction. Shinoda et al. [8] proposed a slip sensor using Acoustic Resonant Tensor Cell (ARTC). The ARTC is composed of a resonance cavity within the elastic body and ultrasonic receiving probe; the slip direction stress is detected from changes in the ultrasonic wave resonance frequency. Ikeda et al. [9] observed the contact surface between an elastic body and a rigid plate by utilizing a camera, and proposed a technique for estimating slip margin. Moreover, various detection techniques have been proposed, such as: sensors simultaneously detecting slip and contact force, by attaching strain gauge to a beam to detect multiple axial forces and moments [10] [11], a micro-heater utilized to heat the tiny area of the object surface; the slip is detected by the change in temperature that occurs at the onset of slip [12], a photo-interrupter embedded in an elastomer; a detector of the oscillation that arises from reflector oscillation between sensor surface and object [13].

However, these sensors had structural complications such as the embedding of a detection device in the finger or requirements for special manufacturing. So there has been the problem of making it small and light-weight. Furthermore, it is necessary to increase the detection elements when sensors utilizing a strain gauge or polyvinylidene fluoride (PVDF) film are arranged over a wide range. With this increase, there is an increase in the amount of wiring and its wiring work is also becomes a problem. This excess wiring is problematic as it becomes a burden on the hand. Accordingly, we carried out this research with the goal of developing a low-profile, light weight slip sensor of simple structure. Hitherto, we have been examining using pressure conductive rubber as the detection element of a slip sensor. Recently, we performed an analysis of the special characteristics of the rubber which indicated the possibility of utilizing it for slip detection [14]. In this paper, first, we will summarize the unique behavior of pressure conductive rubber with regard to shear deformation. Next, we will report the results of the trial manufacture and testing of a slip sensor utilizing these special characteristics. Finally, we will report the results of slip prevention experiments by this prototype slip sensor, and indicate that the pressure conductive rubber is promising as a material of slip sensor.

II. SPECIAL CHARACTERISTICS OF PRESSURE CONDUCTIVE RUBBER

In this chapter, we will discuss the distinctive traits of pressure conductive rubber. A schematic diagram of pressure conductive rubber is shown in Fig.1. The pressure conductive

*Mechanical Engineering and Intelligent Systems, The University of Electro-Communications, 1-5-1 Chofugaoka, Chofu-shi, 182-8585 JAPAN
**Department of Information Physics and Computing, Graduate School of Information Science and Technology, The University of Tokyo, 7-3-1 Hongo, Bunkyo-ku, Tokyo 113-0033, Japan

978-1-4244-2789-5/09/$25.00 ©2009 IEEE

rubber was a high polymer material primarily composed of silicon rubber with carbon particles uniformly distributed within as in Fig. 1-(a). When the pressure was increased, the carbon particles contacted each other as in Fig. 1-(b) forming a conduction route. This appears as a change in electrical resistance. Normally, changes in electrical resistance are utilized in tactile sensors and other devices. However, if pressure conductive rubber that has undergone a vertical displacement then undergoes a shear deformation, the electrical resistance that had decreased up until that point will rise [14]. We consider that this resistance change takes place because of an electric phenomenon by the distribution change of an internal particle. So, We performed the following experiments to research the electrical resistance change generated by shear deformation of pressure conductive rubber.

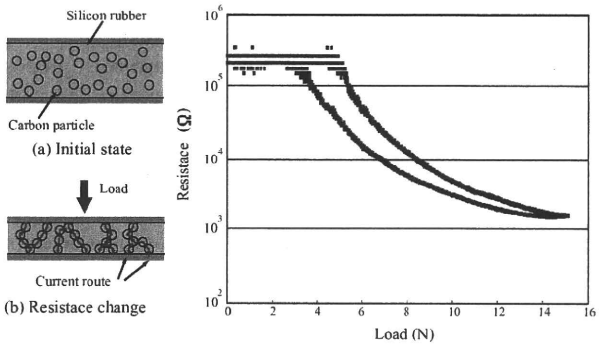

Fig. 1. Model of Pressure conductive rubber and resistance change

A. Experimental Setup

The experimental apparatus is shown in Fig.2. We inserted pressure conductive rubber electrodes, and measured the voltage between electrodes when it was made to undergo a shear deformation. In the experiment, the electrodes (gold plated) were connected to a regulated power supply through a resistance of 1 $k\Omega$, and a voltage of 5 V was applied. The voltage (V_i) was then stable at 5 V. The X-stage installed on the right side of the experimental apparatus was activated, and the normal direction load was increased (Fig.2-(1)). At this time, the voltage between electrodes was decreased from 5 V (load cell output : 0 N) to 2 V (load cell output : approximately 1.7 N). Next, the automatic stage installed on the left side was activated producing a shear deformation of pressure conductive rubber (Fig.2-(2)). The automatic stage had a positioning accuracy of 0.012 mm and its speed could be adjusted from 1 $\mu m/s$ to 100 mm/s. The quantity of the shear deformation of the pressure conductive rubber could be measured by the laser displacement sensor (resolution 0.1 μm). The experimental apparatus was set up to measure voltage change between the electrodes to examine changes in the electrical resistance of the rubber. Experiments were performed regarding the following three items:

- The rubber was made undergo shear transformation, and electric potential between electrodes was observed.
- Measurement was made of changes in electric potential between electrodes when shear transformation speed was held constant and the quantity of shear transformation was changed.
- Measurement was made of changes in electric potential between electrodes when the quantity of shear transformation was held constant and shear transformation speed was changed.

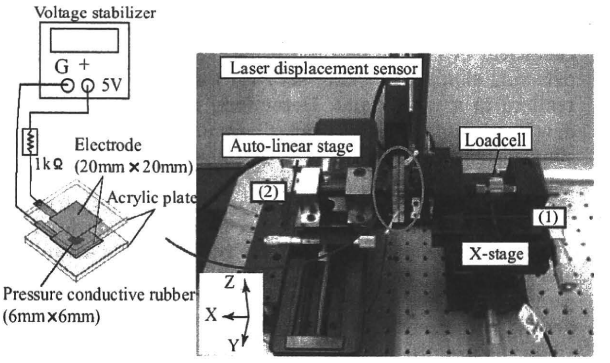

Fig. 2. Experimental equipment

B. Experimental result

Experimental results are shown in Fig.3, Fig.4, and Fig.5. Fig.3 shows the results for a shear deformation of 0.3 mm when the shear deformation speed was set to 0.05 mm/s. The voltage between the electrodes and the quantity of the shear deformation are plotted on the vertical axis of Fig.3. Time is plotted on the horizontal axis. The output of a laser displacement sensor indicated the quantity of shear deformation of the rubber. According to the results of this experiment, there was a rise of 1.5 V in electric potential between the electrodes at the time shear deformation was begun. This result shows that when pressure conductive rubber undergoes a shear deformation, there is a change in electrical resistance. Furthermore, during shear deformation a constant voltage is preserved, and when the deformation halts, the voltage gradually restored to the initial state. Fig.4 summarizes the change in electric potential (ΔV) between the electrodes when the shear deformation speed was held constant at 0.05 mm/s, and the quantity of shear deformation was varied from 0.01 mm to 0.1 mm. The regression line shown on the graph is nearly parallel to the X-axis. That is, the change in electrical resistance of pressure conductive rubber is not dependent on the quantity of the shear deformation over this range. Furthermore, because there was a large change in electrical resistance with a very small shear deformation of 0.01 mm, this shows that this change is highly sensitive. Fig. 5 summarizes the change in electric potential (ΔV) between the electrodes when the quantity of shear deformation was held constant at 0.3 mm, and the speed of shear deformation was varied from 0.01 mm/s to 3 mm/s. The data shows the three measurements that were taken at each speed. The approximate curve is as indicated in the figure, showing that

the change in electrical resistance during shear deformation is dependent on the speed of deformation.

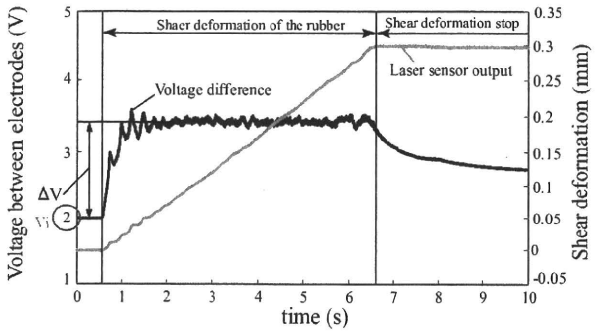

Fig. 3. Shear deformation and Change of voltage between electrodes

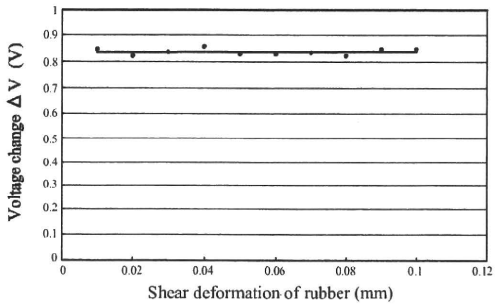

Fig. 4. The quantity of shear deformation and Change of voltage between electrodes

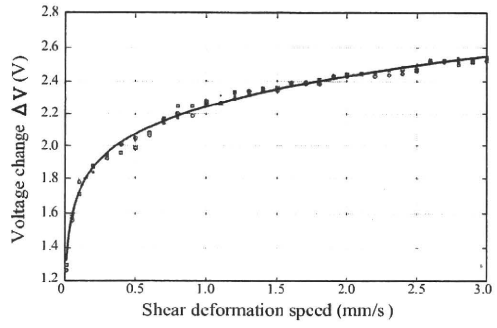

Fig. 5. Shear deformation speed and Change of voltage between electrodes

C. Discussion

In the above situation, in which a constant heavy load causes a shear deformation in pressure conductive rubber, we found an increase in the electrical resistance of the rubber. From experiments varying the quantity of the shear deformation, this change in electrical resistance was found to be caused by a shear deformation as small as 0.01 *mm*, thus it is highly sensitive. From this, it is difficult to assume that volume change produced in the rubber, variation in electrical resistance is produced due to internal changes in the rubber. From Fig.5, we can see that the change in electrical resistance of the rubber depends on the shear deformation speed. Moreover, the voltage produced and the speed of deformation is not linear. In the case of normal direction force, the resistace change depends on characteristics of normal deformation. So, the resistace change by shear deformation also depends on defomation characteristics of pressure conductive rubber. That is, in the case of a slow shear deformation, the internal state of the rubber also changes slowly. On the other hand, when a quick shear deformation occur, it is assumed that there is a sudden change in the internal state of the rubber. Therefore, the change in electrical resistance becomes greater. However, a more detailed examination of the cause which this resistance change occurs is necessary in the future.

III. Application to Slip Sensor

From the above results we believe that the special characteristics of pressure conductive rubber may be put to practical use in slip sensors. Namely, that just before an object slips over a sensor, there is a shear deformation in the pressure conductive rubber. By measuring the change in electrical resistance produced by this shear deformation, we anticipate that the initial stage of slip can be detected. This chapter discusses the manufacture of a prototype of a slip sensor utilizing pressure conductive rubber and the results of slip detecting testing performed.

A. Prototype of Slip sensor

The slip sensor that was trial manufactured is shown in Fig.6. In the configuration of the slip sensor, two electrodes are alternately coiled around a spiral structure, and on the electrodes rests pressure conductive rubber (6 *mm* × 6*mm*). The electrode is connected to a DC power output (5 *V*) through a resistance of 1 *k*Ω. Since this sensor utilizes rubber, it is flexible, light weight, and low-profile (0.5 *mm*). We estimate that the minimum size of this sensor is 3 *mm*× 3 *mm*× 0.5 *mm*. Moreover, As an amplifier circuit is not needed, it is an extremely simple structure.

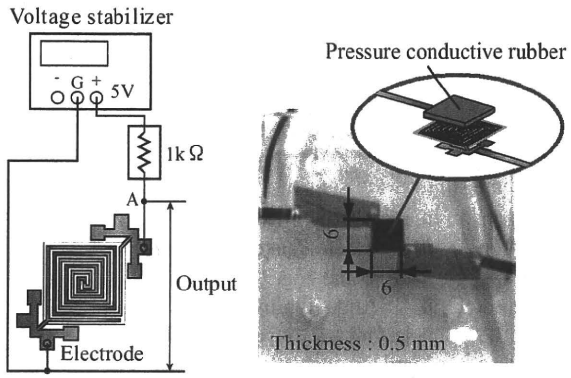

Fig. 6. Prototype of slip sensor with pressure conductive rubber

B. Slip Detection Experiment with Prototype Sensor

In this experiment, we performed to observe the force acting on a prototype sensor and the sensor output change, and to inspect its practical applicability as a slip sensor.

The experimental apparatus is shown in Fig.7. The sensor was deployed within the area of the figure encompassed by the square line, and an acrylic plate was arranged on the opposite side of the slip sensor. The acrylic plate was made slide in the -X direction after pressing on the sensor surface. The acrylic plate was held in fixed position on an automatic stage, and slip could be caused at a constant speed. A six axis sensor was attached to the back of the slip sensor, so measurement of the force acting on the slip sensor was made possible. Measurement of the acrylic plate displacement was made possible by means of a laser displacement sensor (resolution: 0.1 μm) inside the experimental apparatus. For this experiment, the force used to make the acrylic plate slip over the sensor was approximately 2 N, the rate of slip was 0.5 mm/s, and the slip displacement was 4 mm. Measurements were taken in the prototype sensor output, the six axis sensor output, and the laser displacement sensor output.

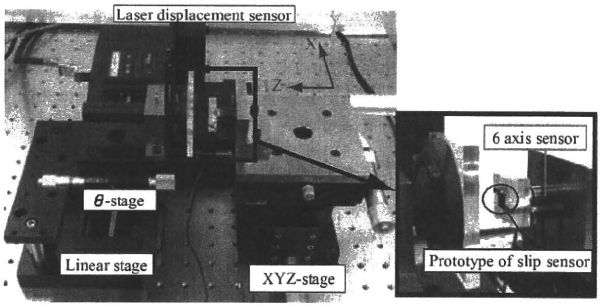

Fig. 7. Experimental apparatus for slip detection experiment

C. Experimental result

The experimental results are shown in Fig.8. Fig.9 shows a graphical enlargement of the interval from 0 seconds to 1 second of Fig.8. In both figures, the upper graph shows the prototype slip sensor output, the middle graph shows the differential of prototype slip sensor output, and the lower graph shows the laser displacement sensor and six axis sensor outputs. The F_z of the lower graph is the load output of the six axis sensor in the Z direction and the force of the acrylic plate pressing on the sensor. F_x is the load output of the six axis sensor in the X direction, indicating the force in the direction (X) that was to make the acrylic plate slip.

Firstly, looking at the Fig.9, the F_z output was a constant value set to 2 N. And, it remained approximately constant from the point before the onset of slip until the end of slip. On the other hand, F_x increased until about 0.4 (s), and then remained at a constant value. That is to say, until 0.4 (s) it was an area of static friction, and thereafter it became an area of kinetic friction. Therefore, the slip between the acrylic plate and the slip sensor was produced on and after 0.4 (s). According to this graph there was a sharp change in slip sensor output produced approximately 0.3 (s) before the onset of slip. At the point when it reached its first peak value, the laser displacement sensor output was 0.01 (mm) or less. After this value reaches its greatest point in the middle, it maintains a nearly constant value with complicated voltage change. From the special characteristics of pressure conductive rubber, it appears that there is a shear deformation produced in this area of the rubber in the direction of slippage.

Next, after the onset of slip, small signs of incidences of slip occurred in several places as shown in the graph in Fig.8. This also slightly appeared in the F_x output, and the timing was coincident. Therefore, we believe that we detected the sticking and slip produced between the acrylic plate and the surface of the slip sensor, namely, the stick-slip of the objects.

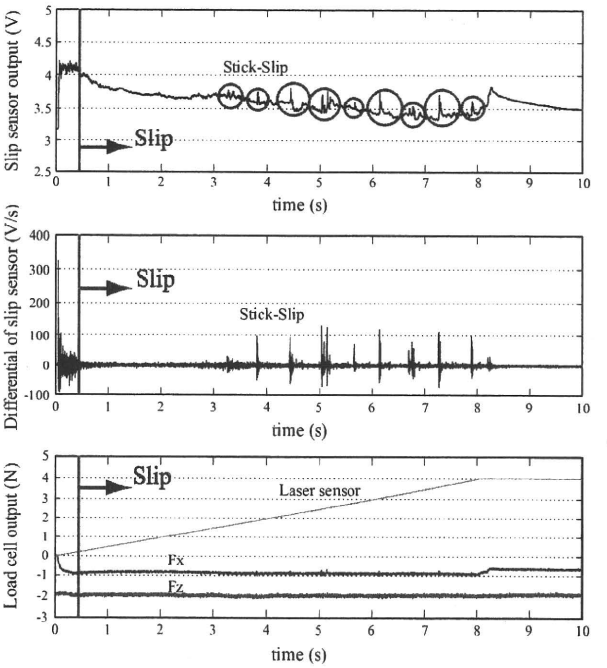

Fig. 8. Slip detection by using prototype sensor

D. Discussion

This output change produced when an object slipped over the slip sensor was due to special characteristics of the pressure conductive rubber. From approximately the interval from 0.05s to 0.4s, the output value remained nearly constant, with the complicated voltage change, as shown in the colored area of Fig.9. The laser displacement sensor output variation over this interval was 0.2 mm. We can assume that the pressure conductive rubber was undergoing shear deformation at this time, thus producing the change. And, this complicated voltage change becomes clear when we examine the sensor output differential value (Fig.9-middle graph). Therefore, it appears possible to adjust the grip force to prevent slip before it occurs, by utilizing the fact that the complicated voltage change is produced just before the occurrence of slip. Accordingly, the following experiments were performed.

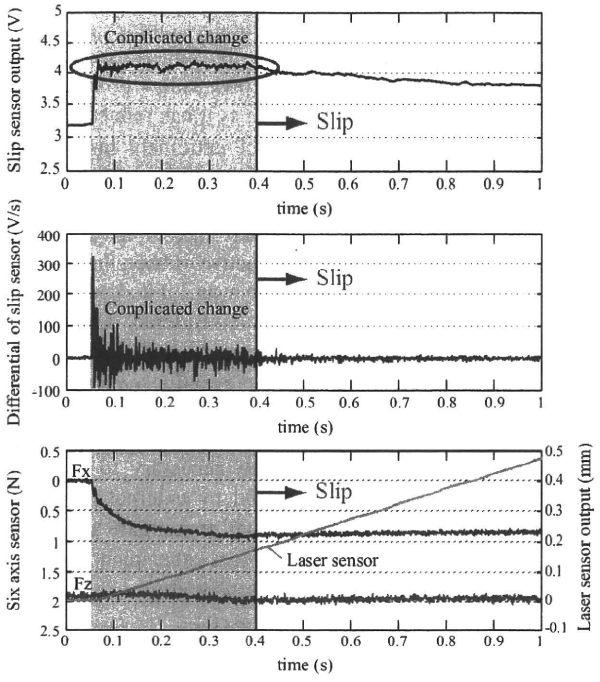

Fig. 9. Output change between 0 (s) and 1 (s)

IV. Slip Prevention by Prototype of Slip Sensor

From the results shown in the prior chapter, detection of initial stage slippage appeared possible by focusing on the output change of the prototype slip sensor produced in the initial stage of slippage. In this experiment, the object slip was detected utilizing the differential value of prototype slip sensor output, and this information was fed back to the auto-linear stage, and the slippage of the object was prevented.

A. Experimental setup

The experimental apparatus utilized in these experiments is shown in Fig.10. The prototype of slip sensor was deployed on the horizontal plane. Above the sensor was placed an acrylic plate of 3 *mm* in thickness, which was sandwiched between the load cell above and sensor below. The load cell was attached to the automatic Z stage, and by the movement of the stage, it was possible to apply any grip force to the acrylic plate. The acrylic plate was connected by wire through a pulley to a cup-like container. To create slippage, a transverse load could be applied to the acrylic plate by putting weights into this container.

That is, an algorithm was used to monitor the sensor output differential value just before the occurrence of slip displacement and move the stage a fixed amount if the value exceeded the threshold, thus increasing the grip force. The threshold of $\pm 5\ V/s$ was established in this experiment by comparing the change in sensor differential values when slippage was produced with when no slippage occurred. The sampling cycle of the slip sensor was 1 *ms*, and the control cycle of the automatic stage was 10 *ms*. After a small grip force (approximately 1.5 *N* in this experiment) was applied to the acrylic plate, weights of 50 *g*, 100 *g*, and 150 *g* were placed into the container, and measurements were made of prototype slip sensor output, grip force change, and displacement of the acrylic plate from the time the container was gently released.

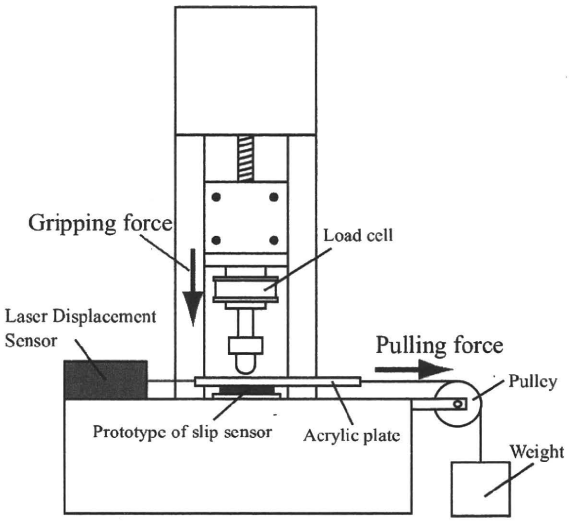

Fig. 10. Experimental equipment for slip prevention experiment

B. Experimental result and Discussion

The results of 100 (*g*) are shown in Fig.11. The upper graph indicates the prototype slip sensor output, the middle graph shows the sensor output differential value, and the lower graph displays the load cell output, and the laser displacement sensor output (resolution: 0.1 μm). From this data, we found that when the slip sensor differential value exceeded an established threshold, the grip force (load cell value) was restored. In each case, no slippage visible to the naked eye was produced. That is, it was possible to prevent slippage for three different types of transverse loads applied. Table I summarizes the convergent load cell value (grip force) and the displacement quantity of the acrylic plate as measured by the laser displacement sensor. It is apparent that the quantity of the displacement increased with each increase in the transverse load, and the grip force utilized also increased. Adjustment of the grip force was realized in response to the weight of the load.

In this experiment, there was not the sharp change in slip displacement immediately prior to the onset of slippage as was the result obtained in the prior chapter (Fig.8-upper graph). This is attributable to the fact that the transverse load was applied slowly and produced a slow shear deformation of the rubber. However, if the transverse load were to be applied suddenly, there would be a sharp change as seen in the preceding section. The sudden addition of a transverse load is the cause of greater slippage, and in such a case, action that prevents slippage is possible through utilization of the change.

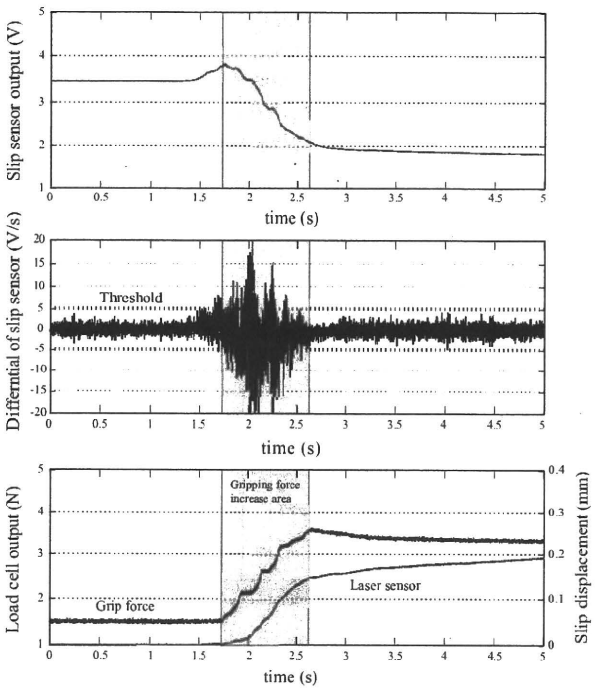

Fig. 11. The object weight is 100 (*g*)

TABLE I

GRASPING FORCE AND DISPLACEMENT FOR OBJECT WEIGHT

	Weight		
	50(g)	100(g)	150(g)
Displacement (mm)	0.12	0.18	0.25
Grasping force (N)	2.6	3.3	4.2

V. SUMMARY AND FUTURE WORKS

We manufactured a prototype of a slip sensor utilizing the special characteristics of pressure conductive rubber and performed experiments in which an object was made slip over the sensor. We were able to find the following results:

- It was found that slip sensor output rose just before onset of slippage, and complecated output change was produced. Detection of the initial stage of slippage (slip prediction) was possible due to these factors.
- There was a small change in slip sensor output over the interval where slippage was produced. This was attributable to the detection of stick-slip produced between the sensor and the object.

We also performed experiments in which the initial stage of slippage was detected utilizing the change in prototype slip sensor output, and a simple algorithm was used to prevent object slippage. As a result, we were able to prevent slippage for the three quantities of transverse load applied. Moreover, the convergent grip force value varied with the size of the transverse load, and the feasibility of grip force adjustment in response to a transverse load was shown.

Existing slip sensors are structurally complex and difficult to install in small areas such as the fingertips of a robotic hand. The slip sensor that we propose is low-profile, flexible, and extremely simple in structure as it has rubber as its main constituent. Furthermore, it is of extremely high sensitive with regard to the detection of the initial stage of slippage.

Hereafter, we will investigate how the slip sensor output changes with differences in such factors as the type or sensitivity of the pressure conductive rubber. In this paper, the object which was made slip was limited to an acrylic plate and other objects were not considered. Therefore, we will examine the effects of differences in object surface and friction coefficient. In our slip prevention experiments, we made use of the simplest method of utilizing the prototype slip sensor differential value. However, when it is practically used as a slip sensor, it will be necessary to isolate this value from output change caused by external forces other than slippage. Accordingly, we will investigate an algorithm to separate the disturbance of forces other than slippage by the combination with the force sensor etc.

REFERENCES

[1] R.S. Johanson, G. Westling, *Roles of glabrous skin receptors and sensorimotor memory in automatic control of precision grip when lifting rougher or more slippery objects*, Exp Brain Res, Vol.56, pp. 550-564, 1984

[2] R.S. Johanson, G. Westling, *Signals in tactile afferents from the fingers eliciting adaptive motor responses during precision grip*, Exp Brain Res, Vol.66, pp. 141-154, 1987

[3] M.R. Trembly, M.R. Cutkosky *Estimating Friction using Incipient Slip Sensing During a Manipuration Task* , Proc. IEEE Int. Conf. on Robotics and Automation, pp.429-434, 1993

[4] J.S. Son, E.A. Monteverde and R.D. Howe, *A Tactile Sensor for Localizing Transient Events in Manipulation*, Proc. IEEE Int. Conf. on Robotics and Automation, pp.471-476, 1994

[5] T. Maeno, K. Kobayashi, N. Yamazaki*Relationship between Structure of Finger Tissue and Location of Tactile Receptors*, JSME Trans, Series C, Vol.63, No.607, pp.881-888, 1997(in Japanese)

[6] Y. Koda, T. Maeno, *Grasping Force Control in Master-Slave System with Partial Slip sensor*, Proc. IEEE/RSJ Int. Con. on Intelligent Robots and Systems, pp.4641-4646, 2004

[7] T. Maeno, S. Hiromitu, T. Kawai, *Control of Grasping Force by Detecting Stick/slip Distribution at the Curved Surface of an Elastic Finger*, Proc. IEEE Int. conf. on Robotics and Automation, pp.3895-3900, 2000

[8] H. Shinoda, S. Sasaki, K. Nakamura, *Instantaneous Evaluation of Friction based on ARTC Tactile Sensor*, Proc. IEEE Int. Conf. on Robotics and Automation, Vol.3, pp.2173-2178, 2000

[9] A. Ikeda, Y. Kurita, J. Ueda, Y. Matsumoto, T. Ogasawara, *Grip force control for an elastic finger using vision-based incipient slip feedback*, IEEE/RSJ Int. Conf. on Intelligent Robots and Systems, pp.810-815, 2004

[10] N. Saito, T. Satoh, H. Okano, *Grasping Force Control in consideration of Translation and Rotational Slippage by a Flexible Sensor*, IEEE Annual Conf. on Industrial Electronics, pp.3892-3897, 2006

[11] A. Ito, N. Tujiuchi, T. Koizumi, H. Oshima, Y. Nojiri, Y. Tsuchiya, N. Hirama, S. Kurogi, *Development and Structure Evaluation of Small Sensor Element for Distributed-Type Tri-Axial Force Sensor of Robot Finger*, IEEE Int. Conf. on Robotics and Biomimetics, pp.1309-1314, 2007

[12] D. Accoto, F. Damiani, R. Sahai, *A thermal slip sensor for biorobotic applications*, IEEE Int. Conf. on Robotics and Automation, pp.1523-1528, 2007

[13] Shang Zhen-dong, Wang Qunyan, Han Jianhai, Xianhong Xu, *Sliding Sensor and Soft Grasping of Electron Hydraulic Servo Manipulator*, IEEE Int. Conf. on Mechatronics and Automation, pp.1459-1464, 2006

[14] S. Teshigawara, M. Ishikawa, M. Shimojo, *Development of High Speed and High Sensitivity Slip Sensor*, Proc. IEEE Int. conf. on Intelligent Robots and Systems, pp.47-52, 2008

High Sensitivity Slip Sensor Using Pressure Conductive Rubber

Seiichi Teshigawara, Satoru Shimizu, Kenjiro Tadakuma
Ming Aiguo and Makoto Shimojo
Mechanical Engineering and Intelligent Systems,
The University of Electro-Communications,
1-5-1 Chofugaoka, Chofu-shi, 182-8585 JAPAN

Masatoshi Ishikawa
Department of Information Physics and Computing,
Graduate School of Information Science and Technology,
The University of Tokyo, 7-3-1 Hongo, Bunkyo-ku,
Tokyo 113-0033, Japan

***Abstract*— Slip detecting tactile sensors are essential to achieve a human-like gripping motion with a robot hand. In previous researches, we have proposed flexible, thin and lightweight slip sensor utilizing characteristics of pressure conductive rubber. However, It was hard for this sensor to distinguish between the object slip and the normal force change. Therefore, we consider the separative method using high frequency elements generated by object slipping. In this paper, we design the information processing method and developed the sensor detecting both contact and initial slip in high sensitivity and a simple composition.**

I. Introduction

Humanoid robots are researched to assist and support human life at the various research institutions. However, in order to advance the robot to the human living space, there is a need to adapt to its environment. If a humanoid robot thinks about the operation of grasping an object, the robot hand must have many degrees of freedom, and using it, they must be able to grasp a variety of objects and operate them. To do this operation, tactile sensors are required to obtain information such as contact position and contact force, and slip. Especially if robot want to grasp in the minimum force without destroying the object and to operation the object dexterously, the sensation of slip plays an important role[1].

So far, a variety of sensors have been developed such as type of sensors to detect vibration when the slip occurred[2][3], and type of sensors to detect the occurrence of stress and strain change[4][5]. Many types of sensors detect changes which occur just before the slip of an object, or "initial slip". However, these sensors are complex structures and there is a problem of wiring, saving smaller and lighter. Also, as you need to embed inside the sensitive element, we consume time and the cost.

In our laboratory, we propose a thin ($0.5mm$) and flexible slip sensor using pressure sensitive conductive rubber[6]. This sensor uses a peculiar resistance change when shear deformation of the pressure conductive rubber occurs [7]. However, It is difficult to separate a resistance change of the normal force and a resistance change of the object slip. In other words, it is hard to realize the separation with the normal direction force change and the object slip. Therefore, we designed the use of a complicated resistance change immediately before a slip occurs (It is a round part in fig.1).

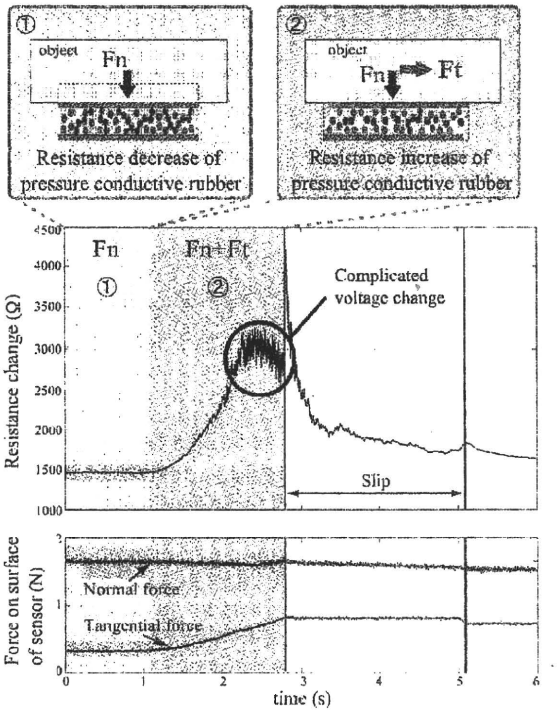

Fig. 1. Resistance change of pressure conductive rubber when object slipped

II. Structure of Slip Sensor

The configuration of this sensor is shown in Fig. 2. In the configuration of the slip sensor, two electrodes are alternately coiled around a spiral structure, and on the electrodes rests pressure conductive rubber ($6mm \times 6mm$). The electrode is connected to a DC power supply ($5V$) through a resistance of $1k\Omega$. Sensor output is a voltage potential between the electrodes(V_{out}). Since this sensor utilizes rubber, it is flexible, light weight, and low-profile ($0.5\ mm$). We estimate that the minimum size of this sensor is $3mm \times\ 3mm \times\ 0.5mm$. Moreover, As an amplifier circuit is not needed, it is an extremely simple structure. Also, the larger the detector plane, saving wiring (just only 2 wires).

978-1-4244-5335-1/09/$26.00 ©2009 IEEE

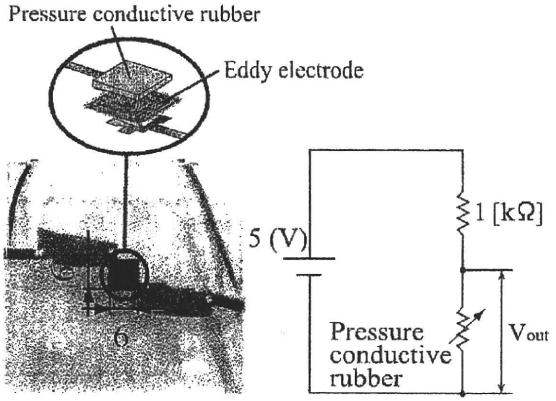

Fig. 2. Structure of slip sensor

III. Slip sensor's output and frequency analysis

We expect that can separate object slip and normal direction force by using a complex change in sensor output when the object slip. Here, we refer to the complex output change for object slip, and result of continuous wavelet analysis to the complicate change. Furthermore, we will compare with a the frequency of the normal force, and describe the difference between the two frequencies.

A. Frequency components when object slip

The experimental apparatus is shown in Fig.3. After we placed the sensor on the horizontal plane, put a acrylic plate on the slip sensor, and add the normal force by using the hemisphere pressure part. We set the normal force to $2N$ by using position control of automatic Z-stage. Next, we installed the wire in the edge of the placed acrylic plate and hitched it to an automatic linear stage through the load cell and slided the acrylic plate on the surface of the sensor. A sliding speed of acrylic plate set to $1mm/s$. Moreover, we measured the slip sensor's output(V_{out}) and the output of the load cell by the sampling frequency $10kHz$.

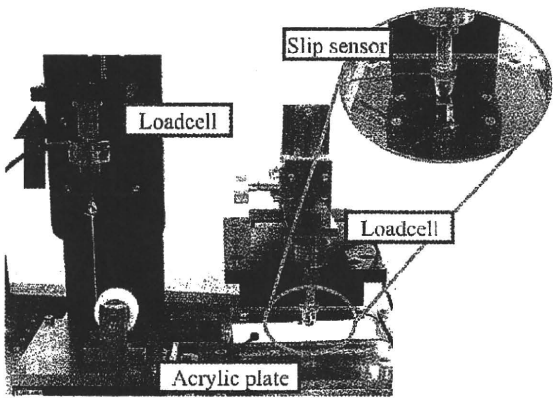

Fig. 3. Experimental apparatus : object slip generator

Experimental data is show in Fig.4. The vertical axis shows the output of the load cell and slip sensor's output and the horizontal axis is time. Seeing a change of tensile force, it increase till $3s$ and it is constant after the time of vertical line. This fact means the change from static friction to kinetic friction. Therefore, the slip between the surface of slip sensor and an acrylic plate are occur from the time of vertical line. On the other hand, looking at the slip sensor's output, it is found that a complex voltage has occurred immediately before an acrylic plate slides.

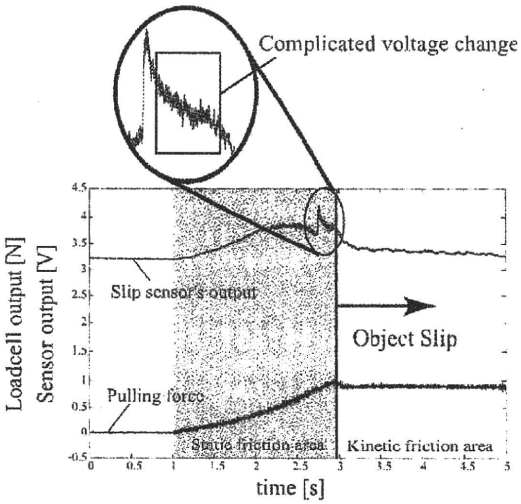

Fig. 4. Experimental results : Output of slip sensor and Tensile force of object

Next, we show the result of a continuous wavelet transform in Fig.5. The upper graph is a change of slip sensor's output, middle graph is a continuous wavelet transform for the upper graph. This vertical axis is "scale" corresponds to the frequency and the horizontal axis is time. Upper side of vertical axis shows low frequency, and lower side is a high frequency. Also, the shade of color shows the power of frequency. Moreover, the bottom three graphs are enlarged graghs of square areas. In the first stage of the voltage change by the tensile force addition, the high frequency component has hardly included and power is also small. On the other hand, we found that the high frequency component increases aiming at immediately before the plate's beginning to slip, and the high frequency of $1kHz$ or more appears. After that, this sensor can detect initial slip by using this high frequency components.

B. Compare with frequency components of normal direction force change

Here, we compare the frequency component by object slip with the frequency component by normal direction force change, and we perform the continuous wavelet transform for output change of normal direction force addition. The experimental equipment is shown in Fig.6. As shown, we

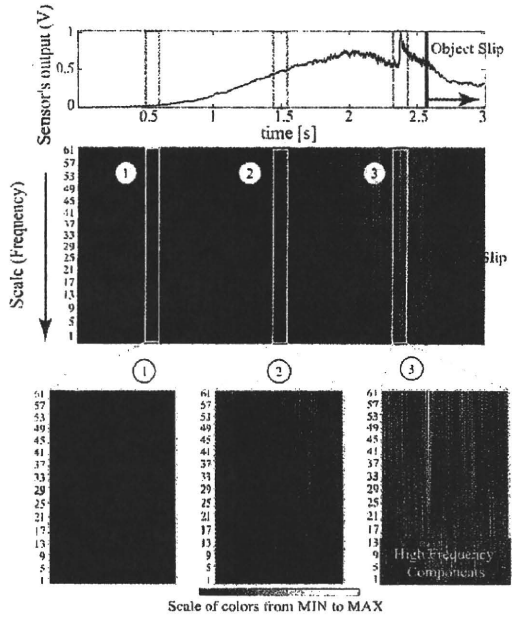

Fig. 5. Continuous Wavelet Transform for the object slip

placed the sensor on a horizontal plane and put $20mm \times 20mm$ acrylic plates on this sensor. Next, we add a perpendicular load to normal direction of the surface of slip sensor using a automatic linear stage. We measured for the output change of the slip sensor at this time and perform continuous wavelet transform to this data.

The result of this experiment is shown in Fig.7. From the result, we found that frequency for normal direction force change is about $600Hz$ at highest. The high frequency component did't appeared when the object slips. From above, it was clarified that the frequency component generated by slip was higher than that by the normal direction force change. Therefore, we can separate these change by using the difference of this frequency components.

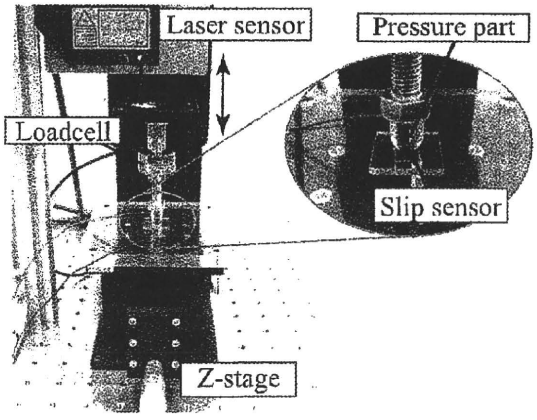

Fig. 6. Experimental Equipment : Adding normal force

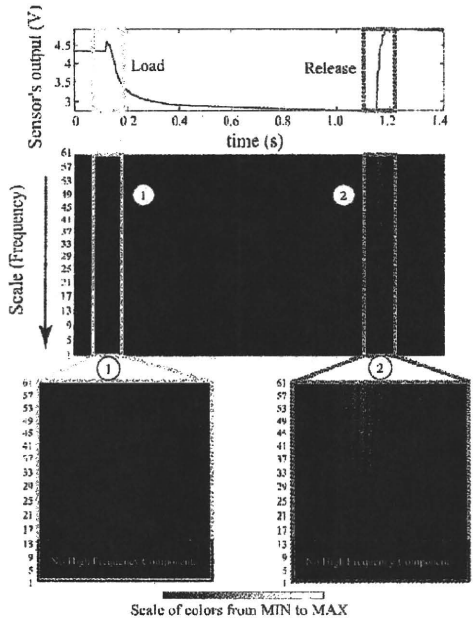

Fig. 7. Continuous Wavelet Transform for the loading and unloading

IV. Separation Method using High Frequency Component

From above, we found that the high frequency component of $1kHz$ or more is included in a complex voltage change when object slip is generated. In addition, it is higher than the frequency when only normal force is added. That is, it seems that it is possible to separate slip and the normal force change by the detection of this high frequency component. Then, we propose the technical way : usage the Discrete Wavelet Transform (As follows : DWT). When perform DWT, the outputs giving the detail coefficients (from the high-pass filter) and approximation coefficients (from the low-pass). This time, we measured the output change of slip sensor under following conditions, and excused DWT of level1 to these data by using the wavelet of Haar.

- Set initial normal force to $2N$, $3N$, $4N$ and slided an acrylic plate (on Fig.3)
- Add normal force on the surface of slip sensor (on Fig.6)

This corresponds to processing that puts the high-pass filter for the output of the slip sensor. Analytical results are shown in Fig.8, 9, 10, and Fig.11. These upper graph is slip sensor's output, and lower graph is DWT for this. As a Fig.11, when normal force change only occur, the wavelet coefficient has hardly changed, On the other hand, from Fig.8 and Fig. 10, it can be observed the wavelet coefficient increase just before object slip occur. Therefore, we can separate the initial slip of the object and the normal force change by setting the threshold to the result of filtering by DWT. Also, there is hardly a difference in the power of the wavelet coefficient when the normal direction power changes as $2N$, $3N$, and $4N$. Hence,

even if the normal direction force changes, we can detect slip of the object by using the same threshold.

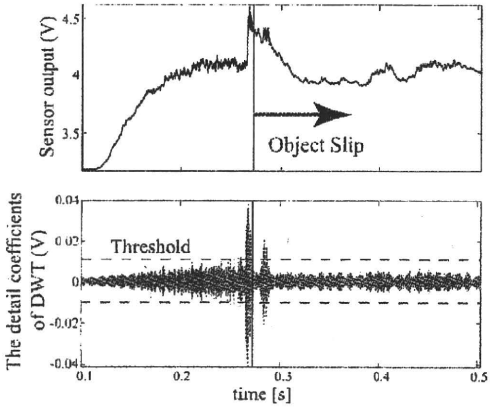

Fig. 8. Analysis results : Discrete Wavelet Transform for the object slip. Initial normal force is $2N$

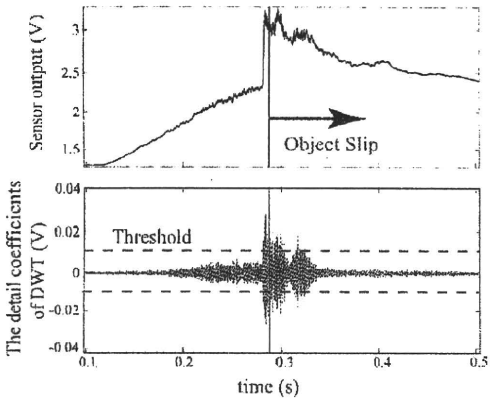

Fig. 9. Analysis results : Discrete Wavelet Transform for the object slip. Initial normal force is $3N$

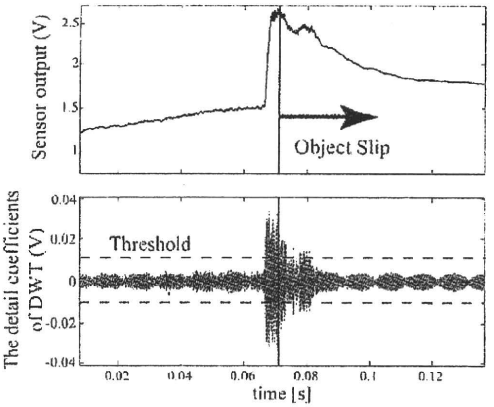

Fig. 10. Analysis results : Discrete Wavelet Transform for the object slip. Initial normal force is $4N$

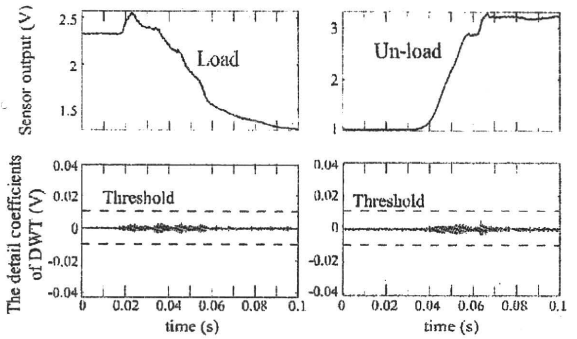

Fig. 11. Analysis results : Discrete Wavelet Transform for the loading and unloading

V. CONCLUSIONS AND FUTURE WORKS

We produce a simple structural slip sensor using the characteristics of pressure conductive rubber. If the object is slided on this sensor, a complex output change occur immediately before the object slip. And, we discovered the high frequency component of several kHz to be contained as a result of analyzing to this output change by using a continuous wavelet transform. In addition, we found that this high frequency component is about one digit higher than the frequency component in the normal direction force change. Then, we proposed the algorithm which separate information of slip from the slip sensor's output change concluded the normal direction force change by using the difference of this frequency component. Here, we extracted the frequency component of slip by using the function of the high-pass filter of DWT. As a result, we found that can separate slip and normal force change by setting the threshold to the detail wavelet coefficient of DWT(level1).

In the future, we verify when the object collides with the surface of the sensor, and will confirm the performance of this slip detection method. In addition, we will research the influence changing the slip velocity and the slip object.

REFERENCES

[1] R.S. Johanson, G. Westling, *Roles of glabrous skin receptors and sensorimotor memory in automatic control of precision grip when lifting rougher or more slippery objects*, Exp Brain Res, Vol.56, pp. 550-564, 1984

[2] J.S. Son, E.A. Monteverde and R.D. Howe, *A Tactile Sensor for Localizing Transient Events in Manipulation*, Proc. IEEE Int. Conf. on Robotics and Automation, pp.471-476, 1994

[3] M.R. Trembly, M.R. Cutkosky *Estimating Friction using Incipient Slip Sensing During a Manipuration Task*, Proc. IEEE Int. Conf. on Robotics and Automation, pp.429-434, 1993

[4] H. SHINODA, K. MATSUMOTO and S. ANDO, *Acoustic Resonant Tensor Cell for Tactile Sensing*, Proc. IEEE Int. Conf. on Robotics and Automation, pp.3087-3092, 1997

[5] K. Noda, I. Shimoyama, *A Shear Stress Sensing for Robot Hands -Orthogonal arrayed Piezoresistive Cantilevers standing in Elastic Material-*, pp.63-66, HAPTICS' 06

[6] S. Teshigawara, K. Tadakuma, A. Ming, M. Ishikawa, M. Shimojo *Development of High-Sensitivity Slip Sensor Using Special Characteristics of Pressure Conductive Rubber*, Proc. IEEE Int. conf. on Robotics and Automation, pp.3289-3294, 2009

[7] S. Teshigawara, M. Ishikawa, M. Shimojo, *Development of High Speed and High Sensitivity Slip Sensor*, Proc. IEEE Int. conf. on Intelligent Robots and Systems, pp.47-52, 2008

速順応型機械受容ユニットへの微小電気刺激により生成される振動感覚に関する検討

Preliminary study of vibration sensation evoked by microstimulation of rapidly adaptive mechanoreceptor units

○鈴木隆文[1)], 矢口博彬[1)], 伊藤孝佑[1)], 滿渕邦彦[1)], 國本雅也[2)]

○Takafumi Suzuki[1)], Hiroaki Yaguchi[1)], Kosuke Ito[1)], Kunihiko Mabuchi[1)], Masanari Kunimoto[2)]

1) 東京大学大学院情報理工学系研究科

2) 済生会横浜市東部病院脳神経センター

1) Graduate School of Information Science and Technology, The University of Tokyo

2) Brain Nerve Center, Saiseikai Yokohama-city Tobu Hospital

我々は感覚神経刺激による触圧覚呈示機能を備えた義手の開発を目指しており、その基礎的研究として、機械受容ユニットへの微小電気刺激によって生成される感覚に関する研究を行っている。今回は、速順応型機械受容ユニットを対象とした実験とその結果について報告する。実験ではまず正中神経へとマイクロニューログラム用タングステン微小針電極を経皮的に刺入し、機械受容ユニットを探索した。皮膚への機械的刺激に対する応答などによって同定したユニットが速順応型であり、かつ、そのユニットへの微小電気刺激によって生成される感覚が振動感覚であった場合に、反対側の手の投射野に対応する部位に実際に機械的振動刺激を加え、その振動周波数を調節するなどの心理物理実験的手法を用いて、微小電気刺激による生成振動感覚の振動周波数を求めることを試みた。結果としては微小電気刺激のパルス周波数と生成振動感覚の振動周波数は概ね一致したが、ときに、後者が前者の半分程度まで小さくなるケースもあった。

P2-9

カフ電極による末梢神経信号データの逐次的信号弁別

Iterative signal classification from neural recordings with cuff electrode

伊藤孝佑 (PY), 山崎博人, 鈴木隆文, 満渕邦彦

Kosuke E. Ito(PY), Hiroto Yamazaki, Takafumi Suzuki, and Kunihiko Mabuchi

東京大学大学院情報理工学系研究科

Kosuke_Ito@ipc.i.u-tokyo.ac.jp

Abstract— Neural Machine Interface (NMI) is a technology that controls the user's movement communicating directly with one's peripheral nerves. For success of NMI with cuff electrodes signal classification from noisy neural recordings is necessarily needed. In this poster we report the method to solve this problem and the results applying it to measurement signals.

Keywords— **Neural prosthesis, sciatic nerve, cuff electrode, signal classification, Neural machine interface**

1 Introduction

近年, 末梢神経より神経情報を取得し, その支配下にある筋骨格部位の運動を補綴する技術 (Neural - Machine Interface, NMI) が研究されている [1]. 現在報告されている限り, これらの研究は神経インタフェースとして, 末梢神経に対し侵襲性の高い構造を持つインタフェースを使用しており, 望ましいとは言えない.

一方で, 実際に臨床の現場で用いられる神経インタフェースとして, カフ電極が挙げられる. カフ電極は機能的電気刺激 (Functional Electrical Stimulation, FES) 等刺激用電極として使用され, また神経に対する侵襲性は低く, 臨床応用に適したインタフェースと考えられる. しかし短所として計測用電極として使用した場合に, 比較的SN 比が低く計測信号の解釈が容易ではない事が挙げられる.

上記の問題を踏まえ, 臨床応用に耐え得る NMI を構築する事を目的とする. 本目的を達成する為には, 以下の様な問題を解決する必要がある: 低 SN 比の計測信号より神経信号及びノイズ信号を選択的に抽出する. 神経信号より遠心性・求心性信号を選択的に抽出する. これらの問題を踏まえ, 我々は遠心性信号と求心性信号が混在する末梢神経信号を伝播方向別に分離するアルゴリズムを考案した. 本発表では, 本手法の概要及び実際にラットの坐骨神経から取得したデータに対し本手法を適用し, 得られた結果について報告する.

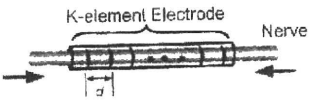

図 1: 仮定した神経インタフェース

2 Methods

末梢神経信号は中枢から末梢へと伝達される遠心性信号と、末梢から中枢へと伝達される求心性信号とに大別される. 前者は運動神経信号及び自律神経信号であり, 後者は感覚神経信号であると見なせる. どちらの信号も非減衰伝播であり, 伝播形状は神経径だけではなく, 計測する電極との距離にも大きく変化してしまう. その為両者を分離する為には, 伝播方向による差異を利用する必要がある. 今末梢神経の走行方向に複数の電極を配置し, 神経信号を取得する事を考慮すると, 各電極における信号の間には伝播遅延が発生する事が分かる. この遅延が伝播速度により異なる事を利用した分離手法を提案した. 以下に概要を記す

2.1 Model

神経信号計測は, 末梢神経束に接して, 軸索の走行方向に対し並行に等しい間隔 d で配置された K 個の電極で行われていると仮定する (図 1). 今, 神経信号を狭周波数帯域 f として伝播速度 v で神経束内を伝播している時, 電極間で得られる信号には $\tau = d/v$ の時間遅延が認められる. その為, 遅延ベクトル $\mathbf{a}(v)$ を $\left[1, \exp\left(-\mathrm{j}\frac{2\pi}{v}df\right), \ldots, \exp\left(-\mathrm{j}\frac{2\pi}{v}(K-1)df\right)\right]^T$, A を $[\mathbf{a}(v_1), \ldots, \mathbf{a}(v_L)]$ を用いて

$$\mathbf{x}(t) = \mathbf{A}\mathbf{s}(t) + \mathbf{n}(t)$$

と表現する. ただし, L は伝播する神経信号群数であ

2.2 Proposed method

2.2.1 Preprocessing

計測データは時間周波数領域へと変換され, 神経信号パワーが集中していると考えられる周波数帯域 $\mathbf{f_m}$ をカベクトル x として用いる.

2.2.2 Estimation of conduction velocities

本設定の伝播速度推定問題は音響学における音源分離法と非常に似通っており，その為伝播速度推定にはMUSIC法[2]を用いた．得られた計測データの自己相関行列$\mathbf{R}_{xx}$を

$$\begin{aligned}\mathbf{R}_{xx} &= E\left[\mathbf{x}(t)\mathbf{x}^H(t)\right] \\ &= \mathbf{A}E\left[\mathbf{s}(t)\mathbf{s}^H(t)\right]\mathbf{A}^H + E\left[\mathbf{n}(t)\mathbf{n}^H(t)\right] \\ &= \mathbf{A}\mathbf{S}\mathbf{A}^H + \sigma^2\mathbf{I} \\ &= \mathbf{E}_\mathrm{S}\mathbf{\Lambda}_\mathrm{S}\mathbf{E}_\mathrm{S}^H + \mathbf{E}_\mathrm{N}\mathbf{\Lambda}_\mathrm{N}\mathbf{E}_\mathrm{N}^H\end{aligned}$$

と固有展開する．遅延ベクトルがノイズ部分空間に直交するという性質から，上記によって得られたノイズ部分空間を張る固有ベクトルを利用して，以下の評価関数

$$P_{MU}(v) = \frac{\mathbf{a}^H(v)\mathbf{a}(v)}{\mathbf{a}^H(v)\mathbf{E}_\mathrm{N}\mathbf{E}_\mathrm{N}^H\mathbf{a}(v)}$$

の極大値を与える伝播速度vを推定速度とした．ただし，神経信号の伝播速度はある範囲に存在するという先験情報を利用して，その範囲内での伝播速度のみを選定する．

2.2.3 Signal separation

推定した伝播速度を用いて，最尤法により

$$\mathbf{y}(t) = \mathbf{s}(t) - (\mathbf{A}^H\mathbf{A})^{-1}\mathbf{A}^H\mathbf{x}(t)$$

と分離される．

2.2.4 Iterative approach

実際MUSIC法を用いて到来方向を予測する為には，ノイズ部分空間行列$\mathbf{E}_\mathrm{N}$が必要であり，それ故相関行列$\mathbf{R}_{xx}$の固有分解を行う必要がある．従って，時間tでの到来方向を推定するにはその時刻の相関行列の固有分解を計算する事が要求されるが，この作業は重度の計算量を必要とすることが知られている．こうした問題に対し，近年のトラッキングシステム分野の研究として，逐次的に信号部分空間を得るBiSVD[3]を用い，逐次的な計算を可能としている．
また同時に，MUSIC法での伝搬速度全域に渡る走査による計算量の増加を防ぐ為，多項式の解に問題を落としたrootMUSIC法を代用している．

2.3 Measurements

末梢神経の神経信号を取得する為，オスのウィスタラット（400~600g）の坐骨神経より，急性実験により麻酔下にて神経信号を取得した．尚，東京大学の動物実験実施マニュアルに従い，動物実験を行った．
露出した坐骨神経に対し，図2の多点カフ電極を用い計測を行った．本電極は神経軸索走行方向に沿う様電極が配置されており，図1に想定する計測環境と一致する．

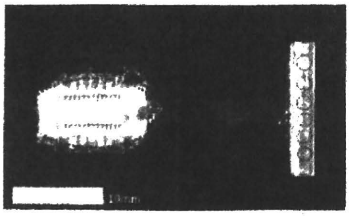

図 2: パリレン製カフ電極

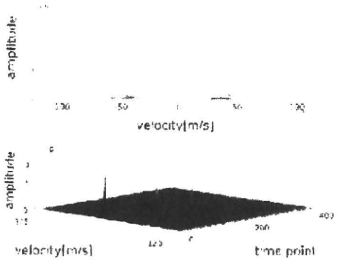

図 3: 実計測信号での伝播速度推定

3 Results

実際にラットの坐骨神経から神経信号を計測し，そのデータに対して本手法を適用した．ラットは麻酔下にあり，運動神経信号が抑制されており，機械刺激により感覚神経信号が伝播されていると考えられる．手法の伝播速度推定では，確かに感覚神経信号と考えられる伝播速度が確認された（図3）．

4 Conclusion

本発表では，臨床応用に耐え得るNMIを構築する前段階として，末梢神経から取得した神経信号の運動・感覚情報の分離方法を提案した．分離手法の評価として，多点カフ電極による実計測信号を用いて本手法へ適用し，その結果として本手法の有用性が示された．今後は慢性下における神経活動計測及び支配下にある末梢部位の運動計測を同時に行い，本NMIシステムの有用性を示していく．

参考文献

[1] G. S. Dhillon & K. W. Horch (2005) "Direct Neural Sensory Feedback and Control of a Prosthetic Arm." IEEE Trans. Neural Syst. Rehabil. Eng., **Vol. 13, No. 4**, 468–472.

[2] R. O. Schmidt (1986) "Multiple emitter location and Signal parameter estimation." IEEE trans. on antennas and propagation. **Vol. AP-34, No. 3.**

[3] P. Strobach (1997) "Bi-iteration SVD subspace tracking algorithms and applications." IEEE trans. on Signal Processing. **Vol. 45, No. 5**, 1222–1240.

平成22（2010）年度

Stochastic estimation of synaptic changes evoked by electrical stimuli in neural network in vitro

Tatsuya Haga, Osamu Fukayama, Takafumi Suzuki, Kunihiko Mabuchi
Graduate School of Information Science and Technology, The University of Tokyo

1.Introduction

Synaptic plasticity contributes to the process of memory and learning in the brain. However, measuring of EPSP as connection strength in large neural network has required great amount of time and work. In this paper, a novel way of estimating synaptic connectivities as a set of parameters of probabilistic neural network model has been developed. The parameters were identified to maximize the likelihood function by assuming spontaneous firings generated from the model. The method was evaluated with a simple simulated neural network, and applied to cultured cell network under electrical stimulus in a Multi Electrode Array Dish.

2.Method

We considered a firing probabilistic model represented by

$$p(x_t^{(i)}=1)=\mathrm{normcdf}(\sum_{j=1}^{N}\sum_{\tau=1}^{T} a_\tau^{(i,j,t)} x_{t-\tau}^{(j)}+\epsilon^{(i,t)},0,\sigma) \quad (1)$$

where $\mathrm{normcdf}(x,\mu,\sigma)$ is cumulative normal distribution function with random variable x, mean μ, standard deviation σ. The number of neuron is N and firing series $x_t^{(i)}$ is 1 when neuron i fires at time t 0 otherwise. synaptic weight at time t from neuron j to neuron i in time-delay τ is $a_\tau^{(i,j,t)}$. Here, $\epsilon^{(i,t)}=\xi^{(i,t)}-\theta^{(i)}$ where $\xi^{(i,t)}$ is the resting membrane potential of neuron i at time t and $\theta^{(i)}$ is firing threshold of neuron i.

Log likelihood fuction for the model at time t is

$$Q_t=\sum_{i=1}^{N}[x_t^{(i)}\log(p(x_t^{(i)}=1))+(1-x_t^{(i)})\log(1-p(x_t^{(i)}=1))] \quad (2)$$

$a_\tau^{(i,j,t)}$ and $\epsilon^{(i,t)}$ can be updated at each time using the gradient method to increase the log likelihood function . The update algorithm is

$$a_\tau^{(i,j,t+1)}=a_\tau^{(i,j,t)}+\mathrm{K}\frac{\partial Q_t}{\partial a_\tau^{(i,j,t)}},\forall i,j,\tau \quad (3)$$

$$\epsilon^{(i,t+1)}=\epsilon^{(i,t)}+\mathrm{K}\frac{\partial Q_t}{\partial \epsilon^{(i,t)}},\forall i \quad (4)$$

where K is the learning coefficient. The synaptic change was estimated in real-time with this method.

3.Experiments

3.1.Estimation in simulated network

The membrane potentials of four Hodgkin-Huxley neurons connected with synapses (Fig.1) are simulated for 20 minutes with a sampling rate of 10 kHz. For the first ten minutes, the EPSC of synapse from cell0 to cell1 was 80nA. During the next ten minutes i.e., 10-20min, this configuration was changed to 160nA. The firing series obtained was then analyzed with our method (K=0.8,σ = 7). Results ($\max_\tau a_\tau^{(1,0,t)}$) are shown in Fig.2. Synaptic potentiation can be seen with convergence interval for about 100sec. The interval may make it difficult to estimate sharp synaptic change.

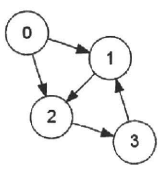

Figure 1: Simulated cell network (node:cell, edge:synaptic connectivity)

3.2 Application to neural network in vitro

We have built a system that can analyze synaptic changes in a neural network in vitro under electrical stimulus such as a single electrical pulse and "the 'Tetenus' " (high-frequency) pulse. The firing series obtained by spike sorting to voltages measured from 8 x 8 electrodes on a Multi-Electrode Array Dish was analyzed to estimate synaptic change. Fig. 3 shows the estimated network as a directional graph.

4.Discussion

While we have found that our method can be used to estimate synaptic changes, slow convergence speed may be a problem. The problem should be solved to apply our methods to various researches to to various researches such as quantitative evaluation of synaptic changes in neural networks in vitro under various conditions of electrical stimulli and in a rat brain with reward learning.

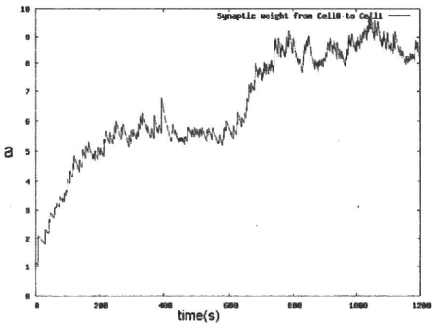

Figure 2: Estimated synaptic weight (cell $0 \rightarrow 1$)

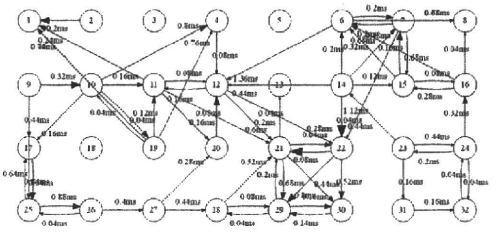

Figure 3: Estimated network

A basic study of kinesthetic feedback by tendon vibration for prosthetic arms

Hiroaki Yaguchi, Kazuki Togawa, Osamu Fukayama, Takafumi Suzuki, Kunihiko Mabuchi
Graduate School of Information Science and Technology, The University of Tokyo

1. Introduction

Kinesthesia is crucial for precise control of the body. A loss of kinesthesia causes ataxia such as unsteadiness in gait and athetosis[1]. In the same vein, prosthetic limbs controlled by neural activities or myoelectric commands require proper kinesthetic feedback for precise control.

A transcutaneous vibration to a tendon non-invasively induces kinesthetic illusion. However, sensations of only small movements were evoked by vibrating a single tendon. We propose the use of a stimulation method in which both ends of each muscle are vibrated to evoke sensations of larger movements.

2. Methods

Twelve healthy volunteers participated in the experiment. Each participant was seated on a chair and held both arms on support tables (Fig.1). The tendons of right biceps brachii and extensor digitorum were vibrated at a frequency of 100 Hz and a peak-to-peak amplitude of about 1 mm. Participants were instructed to show movement velocity they felt in their right arm by moving their contralateral left arm. The intensity of evoked kinesthesia was calculated by subtracting the angular velocity of the right arm from that of the left arm.

2.1 Vibration to biceps brachii

The vibration was presented to both ends of the biceps of 8 participants. While the distal vibration was applied to the tendon, the proximal vibration was applied to the muscle near the muscle-tendon junction because the proximal tendons were behind the other muscles. Vibrations to distal tendon and/or the proximal end were performed 10 times in a random order for a total of 30 trials per participant.

2.2 Vibration to extensor digitorum

The vibration was presented to the distal and proximal tendons of the extensor digitorum of 9 participants. Vibrations to distal and/or proximal tendon of the muscle were performed 10 times in a random order for a total of 30 trials per participant.

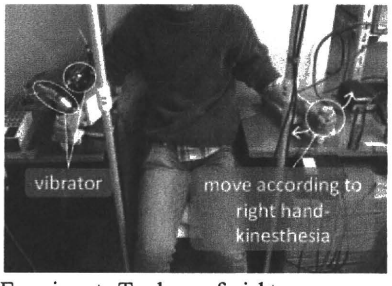

Fig. 1 Experiment. Tendons of right arm were vibrated. Participants moved their left arm to show the velocity of the movement they felt in their right arm.

3. Results and Discussion

Compared to vibration to the distal tendon or proximal end of biceps, vibration to the both evoked a sensation of larger movement ($\alpha = 0.05$, Fig. 2). Similarly, vibration to the both tendons of extensor digitorum evoked a sensation of larger movement than that to the distal or proximal tendon ($\alpha = 0.05$, Fig. 3).

These results may be caused by increasing activity of Ia afferents from the vibrated muscle. Fallon et al.[2] found that only 6 of 32 Ia afferents generated an action potential per cycle when a single tendon was vibrated. Vibration to both ends of a muscle may activate Ia afferents more than that to one end.

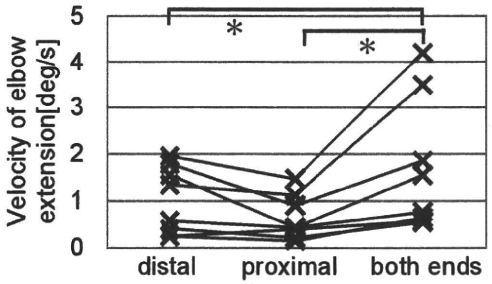

Fig. 2 Mean velocity of illusory movement induced by vibrating biceps. (*: $p<0.05$)

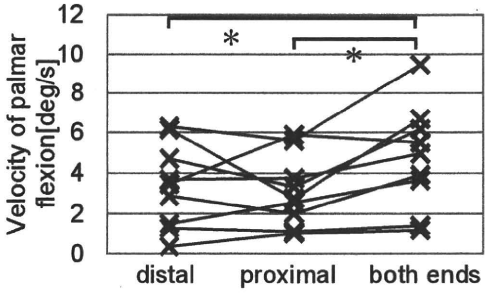

Fig. 3 Mean velocity of illusory movement induced by vibrating extensor digitorum. (*: $p<0.05$)

4. Conclusion

We proposed the use of a stimulation method in which both ends of a muscle are vibrated to evoke sensations of larger movement. Vibration to both ends of biceps or extensor digitorum evoked a sensation of a larger movement than that to a single tendon.

5. References

[1] A. Sghirlanzoni, D. Pareyson and G. Lauria, "Sensory neuron diseases," *The Lancet Neurology*, 4, 2005, pp.349-361.
[2] J. Fallon and V. Macefield, "Vibration sensitivity of human muscle spindles and golgi tendon organs," *MuscleNerve*, 36, 2007, pp.21-29.

6. Keywords

kinesthesia, tendon vibration, non-invasive stimulation

慢性神経信号計測に向けた針型電極の自動位置制御の基礎的検討

柴本 浩児　深山 理　鈴木 隆文　満渕 邦彦
東京大学大学院　情報理工学系研究科

Basic study of automated high-speed positioning of neural electrodes for chronic recording

K.SHIBAMOTO, S.FUKAYAMA, T.SUZUKI, K.MABUCHI,
Graduate School of Information Science and Technology, The University of Tokyo

［はじめに］ブレイン・マシン・インタフェース (BMI) の実用化に向けた重要な課題として、慢性計測における神経信号の安定的な取得が挙げられる。多くの BMI では、脳に針型の神経電極を刺入して計測を行うが、対象の自由行動に伴う衝撃や振動によって電極と脳との相対的な位置関係がずれ、当初計測できた信号を失ってしまうことが問題となっている。本研究では、針電極の埋め込み深さを高速に自動制御することによって、複数の神経細胞と電極との相対的な位置変動に追随可能な慢性計測系の構築を試みる。

［電極埋込深さに応じたスパイク振幅の変化特性］まず予備実験として、ラット海馬に針型電極を刺入し、埋め込み深さに応じた神経発火波形の平均振幅の変化を観察した。その結果、特定の深さに対して再現性良く振幅が最大となり、細胞に最も近接したことが示唆された (Fig1)。

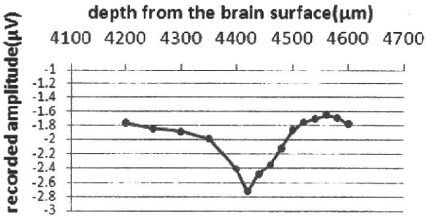

Fig 1: 深度を変化させた時のスパイク平均振幅

［提案手法］前節の予備実験により、計測されるスパイク振幅が連続的に増大するように電極深さを逐次調節することで、電極を神経細胞の近傍に保持できるものと考えられる。複数の神経細胞由来のスパイクが得られる状況 (マルチユニット計測) においては、それぞれの平均高さが指標となりうる。以上を踏まえ、以下のアルゴリズムに従い電極深さを変化させることとした。1）初期位置からスパイクを取得した後、主成分分析を施し、クラスタリングを行う。2）クラスタ中心に最も近い波形をテンプレートとする。3）近傍点を $\pm 2[\mu m]$ とし、そこで得られたスパイクに対してテンプレートマッチングを行う。弁別されたそれぞれのスパイクグループに対し、Negative peak の平均値 $A_i (i = 1, 2, ...)$ を求める。4）評価関数 $J = \sum_{i=1}^{N} A_i$ が前回よりも小さくなっていた場合、それぞれのテンプレートを得られた平均値と一致するような比率で更新し、3）に戻る。それ以外の場合は、何もせず 3）に戻る。ただし、解の探索においては焼きなまし法により局所解を回避した。

［評価実験］ここでは、計算機シミュレーションにより上記アルゴリズムの妥当性を検討した。電極付近の神経細胞を 2 個と設定しそれぞれの深さを 4450μm、4500μm、電極刺入軸との距離を 50μm、60μm とした (Fig2(a))。実験に用いるデータ列は以下のようにして生成した。まずラット海馬から得られた神経スパイクを 2 種類取得し、それぞれ 30〜40Hz、5〜15Hz の頻度で距離の二乗に反比例した振幅で発火させた。次にノイズ用としてスパイクを 50 種類取得し、振幅を 1/8 にした後に 30〜40Hz の頻度で発火させる。深さ 4510μm を初期位置として探索を開始したところ、その推移は Fig2(b) となった。ここで、実線は電極の位置、点線は J が最小となる位置を示す。

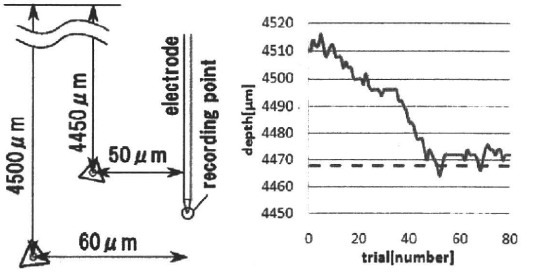

(a)　(b)

Fig 2: シミュレーション

［おわりに］電極と細胞の位置関係によってスパイク振幅の大きさが異なるという予備実験での考察を基に、評価関数を最小にするように電極位置を動かすアルゴリズムの提案を行った。その結果、複数の神経細胞を弁別しながら評価関数が十分に小さくなる位置まで移動することが可能であることが確認できた。今後は、このアルゴリズムの改良と実データでの検証が必要である。

Study on detection and induction of plastic changes in rat brain while connected with a vehicular BMI RatCar

Osamu Fukayama, Takuya Kohama, Takafumi Suzuki, and Kunihiko Mabuchi
Graduate School of Information Science and Technology, The University of Tokyo

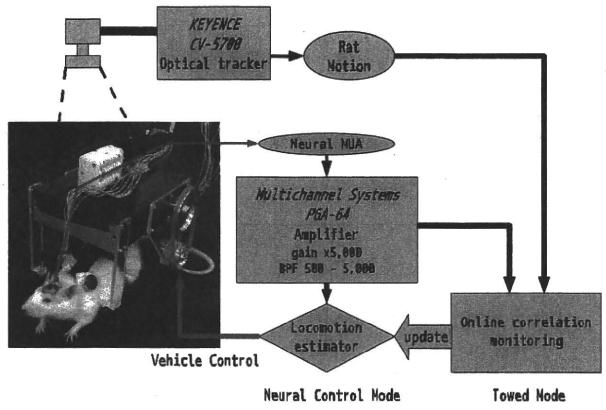

Figure 1: RatCar System operated in 2 modes; neural control mode and towed mode.

1. INTRODUCTION

Brain-machine interfaces (BMI) are promising to provide a new method for device controls. However, brain activities are known to show plastic changes, which disturbs correlating them to a specific motor command. On the other hand, the brain plasticity may assist developing BMIs by adapting the brain with simple neural decoding algorithms which do not initially describe proper neural commands. A vehicular BMI for a rat, which we call "RatCar", has been developed to observe and induce those plastic changes.

2. METHODS

A soft neural electrode made of parylene polymer which had 4 gold recording sites was implanted in the motor cortical regions related to forelimbs of a rat. They were applied to two experiments; controlling a vehicular brain-machine interface ("RatCar"), and forcibly correlating neural activities with a specific action by inducing plastic changes with electrical intercortical micro-stimulation (ICMS).

2-1. Vehicular BMI Control

The RatCar system consists of the neural electrodes described above, an optical motion tracker, locomotion estimators installed on a personal computer, and a vehicle body (Fig. 1).

The system were designed to operate in two modes; "neural control" mode and "towed" mode. In the neural control mode, the vehicle was driven according to extracellular multiunit activities (MUA) patterns recorded from a rat. The rat was suspended under the vehicle as its limbs gently touched the ground. In contrast, in the towed mode, the vehicle was pulled by a rat locomoting with its natural limbs. MUA patterns from the rat brain and motion of the vehicle were simultaneously acquired to identify correlations between the variables. The update process repeated every 100 ms.

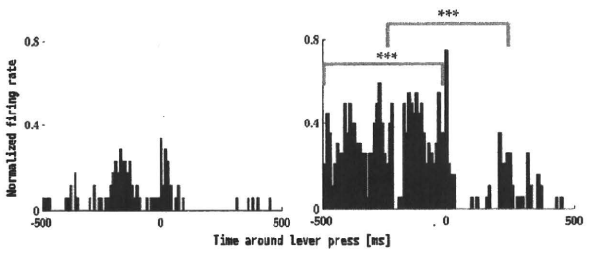

Figure 2: Normalized neural firing rate observed around lever pressing. Pre-stimulation stage (left) and post-stimulation stage (right).

2-2. Correlation Forcing

A study to forcibly correlate neural activities near electrodes with a specific motion in an action learning chamber. First, a rat with neural electrodes implanted in its forelimb region of the motor cortex was trained to push a lever to gain food rewards. Then, a channel was chosen which had initially no strong correlation with the motion (i.e., lever pushing), and ICMS was applied to the channel to induce correlation with the lever pushing motion.

All the experiments we performed followed guidelines given by the "Animal Experiments Committee of the University of Tokyo".

3. RESULTS

The vehicular BMI system operated online; (a) determining vehicle motion in the neural control mode, and (b) monitoring the correlation between neural activities and locomotion of the rat in the towed mode. Properties of those correlations and determination results depended on incidentally recorded neurons.

Then, the correlation forcing method was applied. Normalized neural firing rates increased in prior to lever pushing by the ICMS (Fig. 2), which resulted in stronger initial correlation between a recorded neurons and motor commands related to limb control.

Combination of those methods are promising to detect and apply brain plasticity for a precise BMI.

4. KEYWORDS

Brain-machine interface, Brain plasticity, Locomotion estimation, Extracellular recording, Rat

Development and characterization of flexible L-glutamate biosensor

Naoki Kotake, Takafumi Suzuki, Osamu Fukayama, Shoji Takeuchi, Kunihiko Mabuchi
The University of Tokyo

1. INTRODUCTION

One of the main excitatory neurotransmitters in the mammalian brain, L-glutamate (Glu), is involved in most aspects of normal and abnormal brain function. Previous studies have reported several types of sensors that detect the concentration of Glu in the brain. These sensors consist of a rigid material such as silicon or ceramic [1-2], which does not deform in the brain and consequently damage surrounding tissues when the body moves. We propose the use of a flexible sensor that can fit the brain.

2. METHODS

Sensor fabrication. We used MEMS technology to fabricate the sensors that consist of a parylene thin film structure and four-channel recording sites. A gold layer was deposited and patterned on the first parylene layer. The structures of sensors were then defined by oxygen plasma etching after second parylene layer deposition. After peeling the sensor from the wafer, Nafion was coated on each recording site to repel anions such as ascorbic acid. Glutamate oxidase (GluOx) was immobilized onto the surfaces of two recording sites by coating with bovine serum albumin (BSA) and glutaraldehyde. Others were coated with BSA and glutaraldehyde mixture without GluOx. The sites immobilized by GluOx and ones coated with only BSA worked as Glu detectors and control sites, respectively.

Electrochemical measurements. Detection tests of Glu concentration were done in vitro using constant-potential amperometry. We used a fabricated sensor, a platinum counter electrode, and an Ag/AgCl reference electrode. These electrodes were placed in a continuously stirred 0.1 M phosphate buffered solution (pH 7.4, 37 °C), and operated the sensor at a constant potential of +0.7 V vs. Ag/AgCl reference electrode.

3. RESULTS

A raw current-time response of the fabricated sensor is shown in Figure 1. We consecutively injected Glu using a micro-pipette at the points of time indicated by the arrows (final concentration

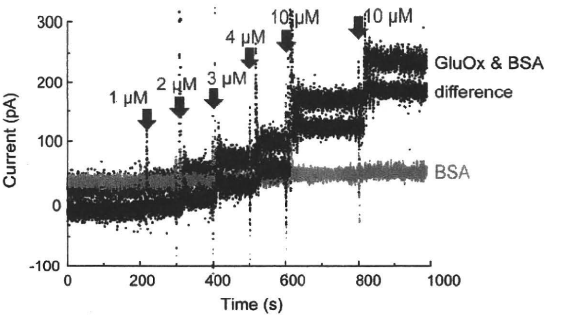

Fig. 1. Response for consecutive Glu injections.

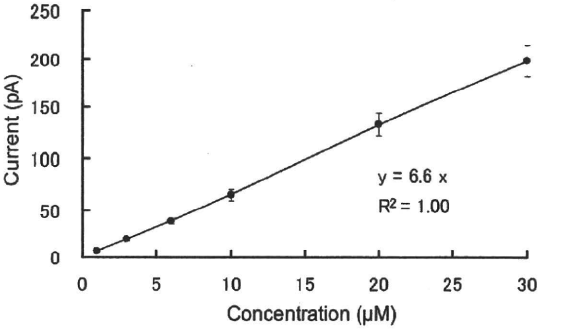

Fig. 2. Calibration curve of sensor.

was 30 μM). The response of the sensor was stable and the response time was within 20 s. The current response of sensor showed the linear response to Glu concentration in the whole measurement range (Fig. 2). The sensor sensitivity calculated from the slope was 6.6 pA/μM, and the linearity (R^2) was 1.00 (n=8).

4. CONCLUSION

We proposed and fabricated a flexible microsensor for detecting the concentration of Glu. The results of in-vitro measurement show that the sensor showed good linearity in the calibration test and could be used at a concentration of under 30μM Glu.

5. REFERENCES

[1] O. Frey, et al., Conf. Proc. IEEE Eng. Med. Biol. Soc., pp. 6040-6043 (2007)

[2] J. J. Burmeister et al., J. Neuroscience Methods 119, p. 163-171 (2002)

6. KEY WORDS

Flexible, sensor, L-glutamate, Neurotransmitter, Parylene

Estimation of finger movements by electromyographic signals with external triggers for playing trumpet

Yutaro Kobayashi, Osamu Fukayama, Takafumi Suzuki, Kunihiko Mabuchi
Graduate School of Information Science and Technology, The University of Tokyo

Key words
Prosthetic arm,
Surface electromyographic (sEMG) signals,
Principle Component Analysis (PCA)

1. Introduction

Electromyographic (EMG) signals have been used to control active prosthetic arms for amputees. One of the obstacles in achieving such prosthetic arms is the *timed estimation of posture*, because EMG signals and muscle movements are not necessarily synchronized. Therefore, the precision of posture estimation can be remarkably improved by externally providing timing information using body motion. An experimental system for playing the trumpet with surface EMG (sEMG) signals to show the validity of our claim has been developed. The system recorded sEMG signals from forearm muscles of trumpet players. Postures of the hands that push the trumpet valves were estimated using the sEMG signals while the correct timing in which the valves were pushed was provided externally.

2. Method

2.1 Valve patterns of trumpet

Trumpet players make different pitches by pushing the 3 valves in different patterns. The 2nd finger controls the 1st valve (the valve closest to the mouthpiece), and the 3rd and the 4th finger control the 2nd and 3rd valve respectively. There are 7 patterns in which the valves are musically allowed to be pushed. Surface EMG signals was recorded to estimate the postures of the three fingers. The correct timing in which the valves were pushed was also recorded (*timing given externally*).

2.2 Onset detection methods

Selected threshold-based onset detection methods [1] were used to estimate the timing of the valves pushed from sEMG signals. The results were then used to compare with the *timing given externally* (Section 3).

2.3 Feature extraction

Surface EMG signals from 8 electrodes were applied to the subject's right forearm (flexor and extensor muscles), and recorded with the sampling rate of 25kHz. 0.16 second of data, right before the valves were pushed, was extracted. Covariance Matrices were then calculated and used as features.

2.4 Experiment

Four different subjects were asked to push the valves with the following instructions.

(A) push 1st valve *10 times (Fig. 1 color: black)
(B) push 2nd valve *10 times (Fig. 1 color: red)
(C) push 3rd valve *10 times (Fig. 1 color: green)

3. Results and Discussion

The Features of the sEMG signals were investigated by Principle Component Analysis (PCA). Fig. 1 (left) shows the results of a subject analyzed using the timing given externally. Fig. 1 (right) shows the results of the same subject analyzed using the timing estimated by Onset detection method (2.2). These results illustrate the effectiveness of providing timing externally to estimate the postures of the hands.

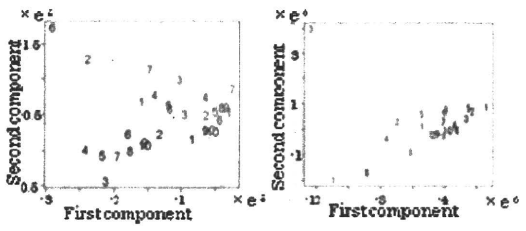

Fig. 1:PCA (left:timing is given externally, right:onset detection method)

*Numerical show the order in which the valves were pushed in each experiment.

Reference

[1]Staude G. et al.:"Onset Detection in surface electro myographic signals," Proc. Journal on Applied Signal Processing, Volume2, pp.67 – 81,2001